Journal of Physics B: Atomic, Molecular and Optical Physics

PAPER

Photoionization dynamics of endohedrally confined atomic H and Ar: a contrasting study between compact versus diffused model potential

IOP Publishing Journal of Physics B: Atomic, Molecular and Optical Physics
J. Phys. B: At. Mol. Opt. Phys. **52** (2019) 145001 (14pp) https://doi.org/10.1088/1361-6455/ab1f16

Photoionization dynamics of endohedrally confined atomic H and Ar: a contrasting study between compact versus diffused model potential

Subhasish Saha[1], Afsal Thuppilakkadan[2], Hari R Varma[2] and Jobin Jose[3]

[1] Department of Physics, IIT Patna, Bihta-801103, Bihar, India
[2] School of Basic Sciences, IIT Mandi, Mandi—175005, Himachal Pradesh, India

E-mail: jobin.jose@iitp.ac.in

Received 13 March 2019, revised 12 April 2019
Accepted for publication 3 May 2019
Published 2 July 2019

Abstract

Photoionization from $H@C_{60}$ and $Ar@C_{60}$ is studied by employing two different model potentials to simulate the endohedral environment. The contrast between the diffusive Gaussian annular square well (GASW) and the compact annular square well (ASW) model potential on the photoionization dynamics is explored by studying the cross-section, phase shift, and Wigner time delay. A realistic description of the fullerene environment requires the right amount of diffuseness and compactness, and the proposed GASW model has both of these attributes. The dynamical properties of an encapsulated atom are studied systematically as a function of the well depth, and it is found that the GASW model induces mild and realistic confinement oscillations on the photoionization parameters in comparison with the ASW case. In addition, the present work brings out a few other interesting features. For a confining well depth of 1.03 a.u., the phase of the dipole matrix elements takes sharp jumps akin to the behavior of dipole phases at the Cooper minimum. In the case of free Ar, the correlation effects contribute less to the time delay in comparison with screening effects near the Cooper minimum. In search of a realistic potential to mimic confinement, the GASW model potential is recommended.

Keywords: photoionization, endohedral confinement, confinement oscillation, avoided crossing, ASW–GASW model potential, Wigner time delay, phase shift

(Some figures may appear in colour only in the online journal)

1. Introduction

The investigation of static and dynamic properties of an atom confined in a C_{60} cage is of particular interest owing to its fundamental and applied nature. On the fundamental side, these studies enable one to understand how trapped atoms respond to external perturbations. From the technological point of view, endohedral systems have promising applications in a wide range of research areas, including quantum computing [1], medical science [2], material science [3, 4], nanoscience and biological science, etc [5–7]. Recently discovered Jahn–Teller metals [8], where a rubidium atom is kept inside the fullerene (C_{60}) shell, exhibit high T_c superconductivity. Zhao *et al* [9] studied novel organometallic molecules based on C_{60}, which are used as a hydrogen (H) storage materials for fuel cell electric vehicles. Confined systems have become an increasingly active area of research because of such exciting applications in various fields of science and technology. Photoionization of an endohedrally confined atom has been the topic of numerous theoretical and experimental investigations [10–12]. These investigations have brought many interesting features, such as confinement

[3] Author to whom all correspondence should be addressed.

oscillations, avoided crossing, and redistribution of oscillator strength [13]. Owing to the difficulty in synthesizing endohedral fullerenes with high yield, most of the earlier works on such systems were essentially theoretical in nature. The scenario has changed in recent decades; Phaneuf *et al* [14] experimentally observed confinement oscillations in the 4d subshell of $Xe@C^{+}_{60}$ ions, thus verifying the theoretical prediction of its existence.

In many of the theoretical studies, the interaction of an electron with the confining shell is simulated by simple model potentials. The annular square well (ASW) potential is the widely used one to mimic confinement effects. Connerade *et al* [15] used the model potential to study the phenomenon of the 'mirror collapse' [15–17] in the vicinity of the avoided crossing between *ns* and (*n*-1) s levels of the H atom. One of the other most employed model potentials for confinement is the δ potential [18]. Amusia *et al* [19] simulated the effects of a confinement cage using a δ-model potential on the 4d, 5s, and 5p generalized oscillator strengths of endohedral Xe, in the energy region above the 4d threshold. Such simpler pseudo potentials employed in previous works can result in a great deal of understanding about the static and dynamic properties of confined systems. Perhaps the most sophisticated theory that included confinement effects was the time-dependent local density approximation (TDLDA) of the density functional theory (DFT) [20]. This method also took care of electron–electron interactions of the C_{60}.

The ASW potential has an unrealistic discontinuity at shell boundaries, which might result in the emergence of artefacts in the calculated photoionization parameters. Replacement of this ASW potential with a more diffused potential like the Gaussian model was explored recently [21]. The confinement is modeled by a smooth attractive short-range spherical Gaussian-type potential to study the electronic structure of $H@C_{60}$ and $H@C_{36}$. [21]. A recent work by Dolmatov *et al* [22] showed clear contrast between the diffuse versus square well potential in modeling confined atoms in the context of photoionization from Xe. The diffuse potential in their work was modeled by a combination of two Woods–Saxon (W–S) potentials, and it was found that the spectra are insensitive to the details of the potential, such as the discontinuity of the potential. Baltenkov *et al* [23] searched for a realistic potential from the point of view of the charge density of the C_{60} shell. The spatial distribution of the positive charge of the C nuclei and negative charge distribution of the electrons of C_{60} were analyzed using Poisson's equation. In contrast to the work of Dolmatov *et al* [22], this work concluded that the often used ASW potential contributed a nonphysical charge density, and hence the ASW potential should be replaced with a more diffused one. These observations mutually contradict some other experimental works that reported that the C_{60} potential has well-defined, compact borders [24].

It is true that confinement will be realistically represented by a potential with diffuse, but compact borders. Hence a search for the right amount of diffuseness and compactness of the confining potential is needed. The objective of the present work is to address the concerns regarding acceptance of diffused versus ASW potentials. To attain this objective, we calculate photoionization cross-sections, phase shift, and time delay of confined H and argon (Ar) by utilizing two different model potentials: the ASW (compact) and the Gaussian annular square well (GASW) (diffused). Several studies suggested that the phase shift and time delay are very much sensitive to confinement, even if the cross-section is not. Therefore, the phase shift and time delay are two important parameters to look at for effects of confinement. These results are compared with existing results [20] in search of a more appropriate potential. These calculations are done in single active electron (SAE) approximations to mask the effects of many-electron correlations, and therefore only effects of confinement will be playing a key role. Otherwise, many competing effects might cancel out the confinement effects and sensitivity to different model potentials will be lost. Hence, this approach is also looking for a realistic confinement potential from the SAE perspective.

While looking for the realistic nature of the confining potential, a method that explicitly includes the position of each C atom of the C_{60} with the correct icosahedral (I_h) symmetry will be an ideal choice. Realistically, the confining 'cage' is more or less penetrable at different locations on this sphere, and hence the spherically averaged model potential used in this work is an added approximation for a less complex calculation. Thus, our conclusions are necessarily qualitative in nature as compared with a real molecular system, which of course would be very much more cumbersome. In addition, lighter atoms have been chosen from the perspective that relativistic effects could thereby be neglected. A proper relativistic treatment requires introducing the large and small components of the 4-wave function and numerical integration of the Dirac equation with a confining potential.

This paper is organized as follows. In section 2 we introduce our model confinement potentials corresponding to a C_{60} cage. Section 3 includes results and discussion, and the work is concluded in section 4.

2. Theoretical details

2.1. Details of model potential

The confining environment of such endohedral systems ($A@C_{60}$) is modeled in this work by two types of potential: (1) the ASW (V_{ASW}) and (2) the GASW (V_{GASW}). In the ASW case, the C_{60} cage is represented by a spherical, short-range, attractive shell potential of mean radius r_c, depth U, and thickness Δ. The ASW model potential is written as

$$V_{ASW}(r) = \begin{cases} -U, & r_c - \dfrac{\Delta}{2} \leqslant r \leqslant r_c + \dfrac{\Delta}{2}. \\ 0, & \text{otherwise} \end{cases} \qquad (1)$$

In accordance with [25], the radius (r_c) and thickness (Δ) of the cage used in this work are 6.7 a.u. and 2.8 a.u., respectively. For the C_{60} fullerene, the depth of the ASW potential ($V_{ASW}(r)$) is modeled such that the electron trapped in the well has a binding energy identical to that of real fullerene,

and its value is accepted to be −0.422 a.u. [19, 26]. However, there are other values also under consideration for V_{ASW}. In the works of Connerade *et al* [27] and Varma *et al* [28], the V_{ASW} is taken as −0.302 a.u., while that in the work of Winstead and Mckoy [29] and Dolmatov *et al* [30] is taken as approximately 0.26 a.u.

$$V_{PN}(r) = \int \frac{n_-(r) - n_+(r)}{|r - r'|} 4\pi r^2 dr' + V_{ASW}(r) - \frac{1}{r}, \quad (2)$$

where $n_-(r)$ and $n_+(r)$ are the ground state electron and proton densities. V_{ASW} is the potential given in equation (1), referred to in the work of Puska and Nieminen [25] as pseudopotential, and is introduced in the well region for quantitative accuracy. In [25], the U in V_{ASW} was appropriately chosen to be 0.7 a.u. so that the binding energy of the valence electrons of the C_{60} cage was in agreement with experimental results [31]. A similar potential is used extensively in the work of Madjet *et al* [32]. In the present work, the potential given by Puska and Nieminen (V_{PN}) in equation (2) is simulated by fitting it with a combination of the ASW potential and Gaussian function:

$$V_{GASW}(r) = \frac{A}{\sqrt{2\pi}\sigma} e^{-\left(\frac{r-r_c}{\sqrt{2}\sigma}\right)^2} + V_{ASW}(r), \quad (3)$$

where A = −3.59 a.u.; standard deviation $\sigma = 1.70$ a.u.; and $r_c = 6.7$ a.u., which is the center of the shell.

V_{ASW} is the ASW potential as given in equation (1), and the value of U is chosen to be 0.7 a.u., in accordance with [25]. The values of Gaussian amplitude and V_{ASW} are chosen such that V_{GASW} qualitatively and quantitatively agrees with V_{PN}. The above-fitted model potential, $V_{GASW}(r)$, thus includes an average effect of 240 electrons and protons of the C_{60} cage and removes the unrealistic discontinuities at the shell boundaries. It is to be noted that equation (2) is now a special case of equation (3) when A = 0. Figure 1 compares V_{GASW} with V_{PN}, and one can see that they qualitatively and quantitatively agree rather well. For a direct comparison, V_{ASW} is also given in figure 1. The present work explores the effect of confinement as the depth of V_{ASW} and V_{GASW} is altered. The V_{ASW} is varied in this work by changing the depth of the potential U. Furthermore, the strength of V_{GASW} (equation (3)) is altered by varying the parameters A and U simultaneously, but keeping the ratio of $\frac{A}{\sqrt{2\pi}\sigma}$ to U fixed to mimic V_{PN} at U = 0.7 a.u. The superposition of the Gaussian and ASW contribution in the ratio of 1.2:1 mimics the characteristic of V_{PN}.

Note also that $V_{GASW}(r_c) = \frac{A}{\sqrt{2\pi}\sigma}$-U is considered as the depth of the potential in the GASW model case. Thus, the GASW model is a parametrically adjustable superposition of the Gaussian and ASW contribution. The model potential V_{GASW}, obtained by fitting the potential in the work of Puska and Nieminen [25], provides a smooth and viable alternative to the V_{ASW}, which has a flat base and sharp boundaries. The advantage of using V_{GASW} instead of V_{PN} is the tunability of parameters to study the effects of confinement as depth varies.

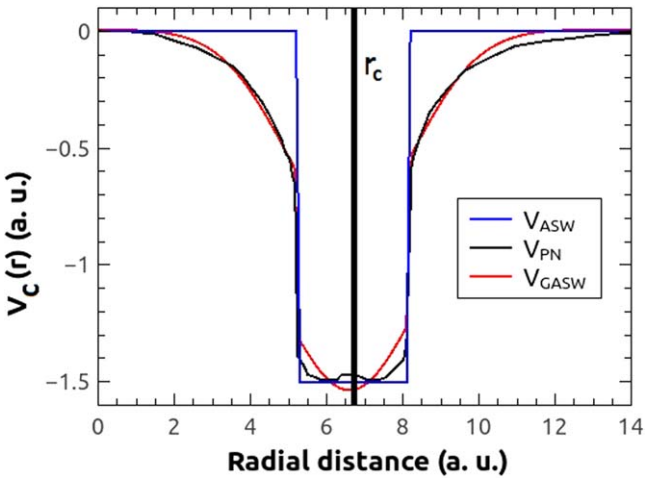

Figure 1. Comparison of the potential V_{GASW} with V_{PN} and V_{ASW}.

2.2. Photoionization

The radial Schrödinger equation of the photoionized electron moving under the influence of a spherically symmetric confinement potential $V_c(r)$ is given by

$$\frac{d^2R(r)}{dr^2} + \frac{2}{r}\frac{dR(r)}{dr} = 2(V_{eff}(r) - E)R(r), \quad (4)$$

$$\text{where, } V_{eff}(r) = \frac{l(l+1)}{2r^2} - \frac{Z_e(r)}{r} + V_c(r). \quad (5)$$

In the above equation, $Z_e(r)$ is the effective nuclear charge, and $V_c(r)$ represents the spherical confinement potential, $V_{ASW}(r)$ or $V_{GASW}(r)$, and R(r) is the corresponding radial wave function. Here, values of l are chosen according to the dipole selection rule. We solve equation (4) using Numerov's method for obtaining the continuum state radial wave function ($R_{El}(r)$) with $E = E_{PE}$ (note the use of atomic units, in which $e = m = \hbar = 1$ throughout the paper) as the photoelectron kinetic energy. The photoionization cross-section (σ_c) under the influence of a linearly polarized electromagnetic field is written as

$$\sigma_c = \frac{4}{3}\pi^2 \alpha E_{Ph} \langle R_{El}|r|R_{nl}\rangle^2, \quad (6)$$

where E_{Ph} is the incident photon energy, and $\alpha(=1/137\ a.u.)$ is the fine structure constant. $R_{nl}(r)$ is the radial bound state wave function obtained by solving equation (4) with binding energy $E = E_b$ and l value corresponding to the initial state. It is to be noted that while solving the radial Schrödinger equation an extra caution is taken to ensure the continuity of the radial wave function and its derivatives at the inner and outer well boundaries [15].

In the case of H@C_{60}, only one (nonrelativistic) dipole transition will occur from the 1s subshell ($1s \rightarrow \varepsilon p$). Equation (4) is solved with $Z_e = 1$ for calculating $R_{nl}(r)$ and $R_{El}(r)$, and thereby the photoionization cross-section is computed. In the case of Ar@C_{60}, we have a different situation as the system is multi-electronic and there are two allowed dipole (nonrelativistic) transitions from the 3p

subshell ($3p \rightarrow \varepsilon d$ and $3p \rightarrow \varepsilon s$). For isolating confinement effects from many-electron effects, the atom is approximated in an SAE model [33]. To solve equation (4) numerically, $Z_e(r)$ is parameterized in the form [34]

$$Z_e(r) = 1 + a_1 e^{(-a_2 r)} + a_3 r e^{(-a_4 r)} + a_5 e^{(-a_6 r)}. \quad (7)$$

The parameters in equation (7) can be obtained by fitting the calculated binding energies from this potential to the experimental binding energies of the ground state and the first few excited states of the target atom. The values of these parameters used in the present work are mentioned in [34].

The dipole matrix element for the transition from the initial bound state ψ_i (3p) of Ar to the final continuum states ψ_f (εs and εd) due to a linearly polarized light field can be written as [33]

$$\langle \psi_i | z | \psi_f \rangle = \frac{1}{\sqrt{3\pi k}} \begin{bmatrix} e^{i(\sigma_0+\delta_0)} \langle R_{31} | r | R_{E0} \rangle / 2 \\ -e^{i(\sigma_2+\delta_2)} \langle R_{31} | r | R_{E2} \rangle \end{bmatrix}, \quad (8)$$

where the partial wave phase shifts δ_0 and δ_2 are associated with the dipole transitions $3p \rightarrow \varepsilon s$ and $3p \rightarrow \varepsilon d$, respectively. Similarly, σ_0 and σ_2 are the Coulomb phase shifts associated with the same transitions. This equation is obtained by writing the initial bound state wave function $\psi_i(r)$ as,

$$\psi_i(r) = \frac{1}{r} u_{nl_i}(r) Y_{l,m_i}(\Omega), \quad (9)$$

where $u_{nl}(r) = rR_{nl}(r)$.

The final outgoing photoionized wave can be expanded in terms of partial waves as follows:

$$\psi_f(r) = \frac{1}{\sqrt{k}} \sum_{l=0}^{\infty} \sum_{m=-l}^{l} i^l \exp[i(\sigma_l + \delta_l)] \times \frac{1}{r} u_{El}(r) Y_{lm}(\Omega) Y_{lm}^*(\Omega_k), \quad (10)$$

where $u_{El}(r) = rR_{El}(r)$, and k is the momentum of the ejected photoelectron electron. δ_l and σ_l are the lth partial wave phase shift and Coulomb phase shift, respectively.

The total photoionization cross-section for the transition from an initial bound state ψ_i to final continuum states ψ_f due to the linearly polarized light field is [33]

$$\sigma_c \propto \frac{1}{k} \left[\frac{|\langle R_{31} | r | R_{E0} \rangle|^2}{4} + |\langle R_{31} | r | R_{E2} \rangle|^2 \right]. \quad (11)$$

2.3. Phase shift and time delay

The focus of this work is to analyze phase shift and time delay in photoionization from confined atoms. The phase shift (δ_ℓ (k)) for a single photoionization channel from H is determined by referring to the asymptotic behavior of the photoelectron wave function [35]:

$$R_{El}(r) \rightarrow \frac{1}{r} \sin\left(kr - \eta * \ln 2kr - \frac{l\pi}{2} + \sigma_l + \delta_l \right), \quad \text{where } \eta = -\frac{1}{ka}; \text{ and } a \text{ is the Bohr radius.} \quad (12)$$

When we have more than one allowed dipole channel, the phase shift is obtained as the phase of the complex matrix element in equation (8).

For the specific case of photoionization from the 3p subshell of Ar, the complex phase shift is written as follows:

$$\phi_c = \tan^{-1} \left(\frac{\sin(\sigma_0 + \delta_0) \frac{\langle R_{31} | r | R_{E0} \rangle}{2} - \sin(\sigma_2 + \delta_2) \langle R_{31} | r | R_{E2} \rangle}{\cos(\sigma_0 + \delta_0) \frac{\langle R_{31} | r | R_{E0} \rangle}{2} - \cos(\sigma_2 + \delta_2) \langle R_{31} | r | R_{E2} \rangle} \right). \quad (13)$$

Having discussed the photoionization phase shift, the time delay is described next. The concept of time delay in the atomic scale was introduced in the early works of Wigner [36] in the context of s-wave scattering. Since photoionization can be viewed as half scattering, the photoionization time delay can be described as a slight temporal delay in the release of the photoelectron wavepacket upon absorption of a short electromagnetic pulse. The time delay in a collision process, defined in terms of an energy derivative of the phase shift, is the same as the collision lifetime. Information of the time delay is extracted from the phase shift of the outgoing electron as follows:

$$\tau_w = \frac{d\delta_l}{dE} \text{ (in the case of H) and } \tau_w = \frac{d\phi_c}{dE} \text{ (in the case of Ar).} \quad (14)$$

The attractive well phase shift is positive, which reveals the pulling of the charged particle within the confinement. However, in the case of a repulsive barrier, the phase shift is negative, which emphasizes the pushing of the charged particle out of the confinement [37]. Based on the nature of the potential, positive and negative time delays are possible. The potentials V_{ASW} and V_{GASW} are employed in this work to systematically study the effect of confinement on the photoionization cross-section, phase shift, and time delay of H and Ar. The results are discussed in the next section.

3. Results and discussion

The attractive potential due to the fullerene cage can be altered in a variety of ways, such as changing the number of C atoms it contains, or adding or removing electrons from C_{60} to make it effectively positive or negative [38]. These alterations can be implemented in a theoretical investigation by changing the depth of the confining well. In the present work, we report the effect on dynamic properties for both H and Ar as the confinement depth at $r = r_c$ varies.

3.1. Photoionization from H@C_{60}

Figure 2 shows the evolution of the wave function of the 1s electron as the depth of the GASW potential is increased. In this case, more electrons are transferred toward the C_{60} shell region, which is quite consistent with the findings reported in [16]. At V_{GASW} (r_c) = 0.56 a.u., mirror collapse happens between 1s and 2s states as a consequence of the 'avoided

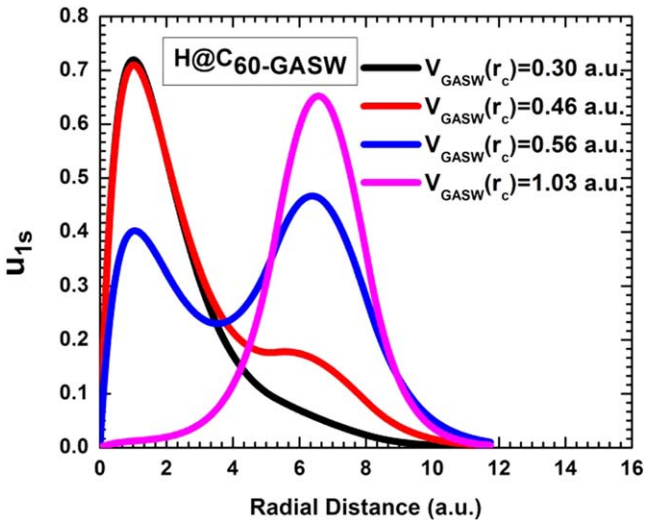

Figure 2. The radial wave function of the 1s electron of confined H for different depths of the GASW potential.

crossing'. Thereafter, the 1s electron density is transferred almost completely to the well region, mirroring the behavior of the 2s electron. The response of the H@C_{60} 1s wave function to the changes in the depth of the ASW potential is qualitatively the same as that in the GASW case but quantitatively different.

In figure 3, the comparison of photoionization cross-sections from the 1s orbital of H@C_{60} using the ASW and GASW model potentials are shown. Here, the ASW cross-section is obtained by switching off the Gaussian part in equation (3) and adjusting the well depth. Also included is a comparison with earlier studies, in which the power exponential [39] form of the potential and the W–S potential [40] are used for confinement. Attributes of the ASW and GASW model potentials are adjusted to those of the power exponential [39] and W–S potential [40] so that a meaningful comparison is possible. It is found that the GASW cross-section is incrementally different in comparison with the ASW and other models. However, the confinement oscillations in the cross-section for the GASW is mild compared to those for the ASW, W–S, and the power exponential because of the combination of both smoothness and compactness at the boundary of C_{60}. Because of these differences, it will be worthwhile to systematically contrast photoionization parameters from ASW and GASW models for different depths.

Figures 4(a) and (b) show the 1s photoionization cross-section as the depth of the ASW and GASW confinement potential is increased. The bare H 1s cross-section is also displayed for comparison. The cross-section exhibits oscillations due to the confinement in both ASW and GASW cases compared to the free H case. As the depth of the confinement is increased, the confinement oscillation is also increased in both cases [39]. For the cases of U = 1.03 a.u. and $V_{GASW}(r_C)$ = 1.03 a.u., the oscillations are not prominent in the scale provided. Figure 4(c) compares the H 1s cross-section for ASW and GASW confinements for two different depths (0.46 a.u. and 0.56 a.u.) with that of free H. The GASW cross-section is seen

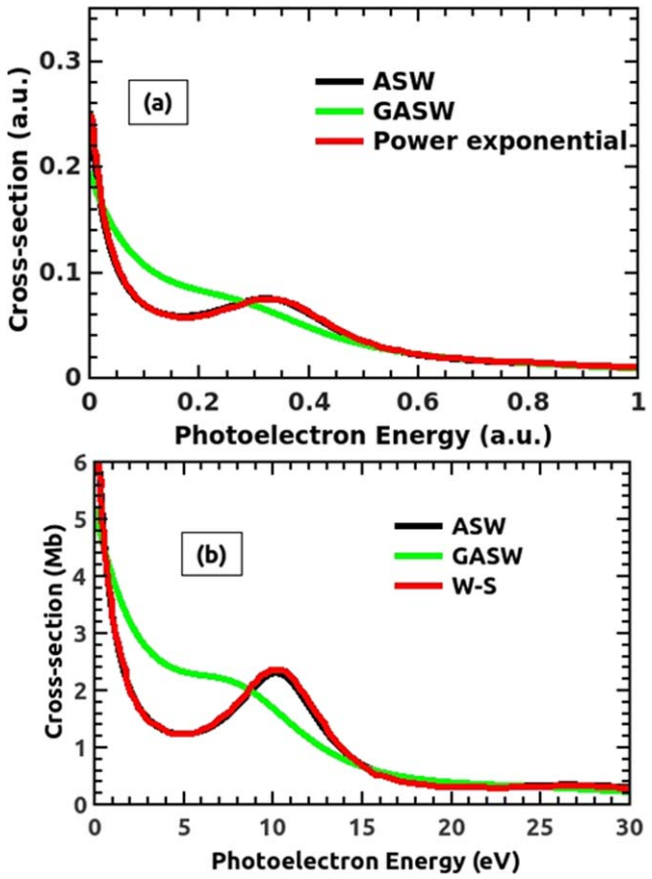

Figure 3. Photoionization cross-section of the 1s subshell of H@C_{60} using ASW and GASW model potentials compared with that employing (a) the power exponential potential [39] with the parameter set at R_{in} = 5.75 a.u., R_{out} = 7.64 a.u., thickness Δ = 1.89a.u., and depth = 0.3028 a.u. (b) W–S potential [40] with the parameter set at R_{in} = 6.01 a.u., R_{out} = 7.26 a.u., thickness Δ = 1.25a.u., and depth = 0.422 a.u.

as less modulated by confinement oscillations than the ASW cross-section. The mellowed behavior of the GASW cross-section is similar for all depths of confinement studied. This behavior seems quite intuitive; however, it has a far-reaching consequence when we compare the ASW and GASW photoionization parameters in search of a realistic potential, which will be unraveled soon.

The threshold behavior of the photoionization cross-section under confinement is quite interesting. Figure 4 shows that, as the confinement depth increases, the cross-section at the threshold decreases (except for the case of the 0.46 a.u. GASW, which will be discussed later). This trend is analyzed in light of the strength of the dipole since the dipole cross-section is primarily decided by the transition matrix element. Table 1 shows the cross-section and the overlap integral near the threshold (E_{PE} = 0.0001 a.u.) as the depth of the ASW and GASW potential is increased. The general trend of the threshold cross-section is to decrease as the strength of confinement is risen. From the overlap integral (table 1) it is noted that the integral is positive in the beginning, and grows negative as the depth is increased. This behavior can be

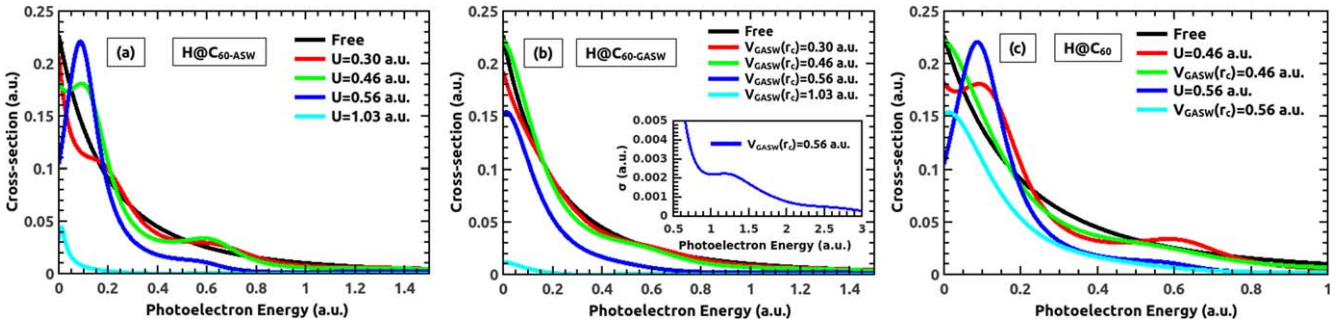

Figure 4. Photoionization cross-section of the 1s subshell of the $H@C_{60}$ atom with (a) ASW confinement and (b) GASW confinement for different depths; (c) comparison of the H 1s cross-section for ASW and GASW confinements for two different depths (0.46 a.u. and 0.56 a.u.) with that of free H. A magnified view of the cross-section is shown in the inset of figure 4(b) for $V_{GASW}(r_c) = 0.56$ a.u.

Table 1. The numerical value of the H 1s cross-section and overlap integral with different strengths of the ASW and GASW model potentials at $E_{PE} = 0.0001$ a.u.

Depth (a.u.)	$s = \int \psi_f \psi_i dr$ ASW (GASW)	σ (a.u.) ASW (GASW)
0	1.082 47	0.224 95
0.30	1.031 56	0.205 20
	(1.020 82)	(0.191 31)
0.46	0.960 23	0.181 49
	(1.082 51)	(0.222 06)
0.56	0.662 91	0.106 54
	(0.749 88)	(0.152 114)
1.03	0.024 69	0.034 92
	(0.011 81)	(0.012 04)

understood if we analyze the constituents of the overlap integral: the initial state and the final state wave functions.

Figure 5 shows the initial state (u_{1s}) and final state ($u_{\varepsilon p}$) wave functions of H and the product of these states ($u_{1s} \cdot u_{\varepsilon p}$) for various depths of the GASW potentials 0.46 a.u. (figures 5(a)), 0.56 a.u. (figures 5(b)), and 1.03 a.u. (figure 5(c)) along with corresponding confining potentials. At lesser depths, the positive overlap contributed by the electron densities near the nucleus results in a cumulative positive overlap integral. As the depth of the potential is increased, the electron density increases in the annular shell region, which is shown in figure 5. At the same time, the electron density decreases near the nucleus as the depth is increased. This culminates into a competition between the gain of the population in the annular shell region against the loss of electron population near the nucleus as the depth is increased. This means that increasing depth results in a decreasing overlap integral, thereby decreasing the cross-section (table 1).

It is clear that the amplitude of the photoionization cross-section at the threshold increased suddenly for the GASW of confinement strength 0.46 a.u., which is comparable to the bare H 1s cross-section. This is on account of the dependence of binding energy on the nature of the confinement. For instance, in the GASW case, the binding energy of the 1s subshell of H is slightly higher compared to that in the ASW case, which is attributed to the diffuseness of the GASW confinement. From this perspective, the photoionization from the ASW- and GASW-confined atoms is much similar than the photoionization from isoelectronic sequence members (neutral atoms and positive ions) where binding energy changes for atoms and ions with the same number of electrons. In such cases, the cross-section tends to follow the profile of the member at the neutral end, with a gentle sweep to the high-energy side as the binding energy increases [41]. This behavior is copied in the 1s subshell cross-section for the ASW and GASW cases with the ASW mimicking the neutral atom behavior and the GASW mimicking that of positive ions. Therefore, the photoionization cross-section for the GASW case is shifted toward the higher-energy region of the corresponding ASW case. On account of this, the GASW cross-section, for the case of 0.46 a.u., missed the minimum and started at the maximum of the oscillation. Apart from this, the threshold behavior is similar for the ASW and GASW: the qualitative nature of the evolution of the overlap integral is the same, but they differ quantitatively.

Having analyzed the threshold behavior, we go ahead to examine the confinement oscillation from a new perspective. Confinement oscillations are reported theoretically and discussed for the first time by Connerade *et al* [42]. The origin of these confinement oscillations in such an endohedral system is due to the interference between three waves: the original outgoing wave and the waves reflected at each of the inner and outer shell boundaries. It was reported by Connerade *et al* [42] that the peak of the confinement oscillation happens when the two returning reflected waves arrive back in phase at the radius of the peak in the initial state wave function. The authors chose an ion as a target to avoid any possible electronic transfer of initial state density into the confining shell. By this, they meant to culminate the effect of confinement mostly on the final state alone.

In this work, we attempt to examine the origin of confinement oscillation using an initial state whose electron density can be transferred to the confining shell region as the well depth is increased. To maximize the effect of confinement, we choose the initial state for a depth of 1.03 a.u., at which the electron density is completely transferred into the confining region, which is followed by mirror collapse with the 2s excited state.

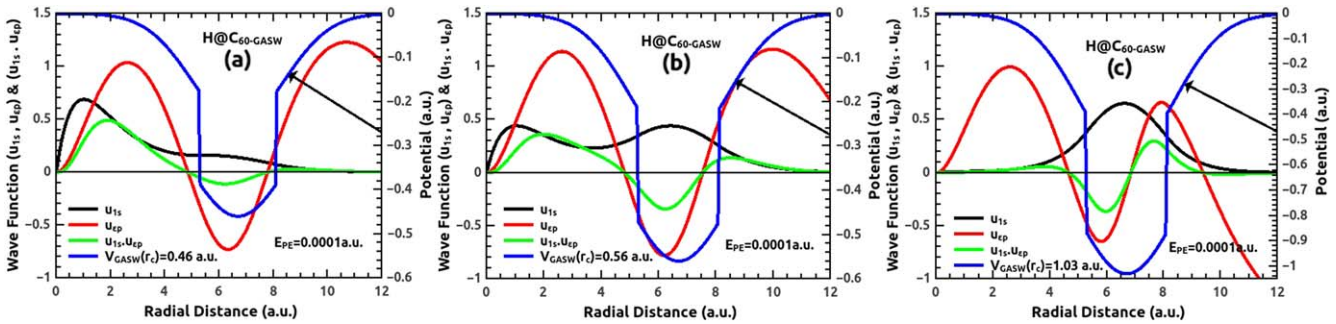

Figure 5. Initial state wave function (u_{1s}), final state wave function ($u_{\varepsilon p}$), and product of the states ($u_{1s} \cdot u_{\varepsilon p}$) of $H@C_{60\text{-GASW}}$ for various depths of confinement (a) 0.46 a.u., (b) 0.56 a.u., and (c) 1.03 a.u. for $E_{PE} = 0.0001$ a.u. (near threshold) along with the corresponding confinement potentials.

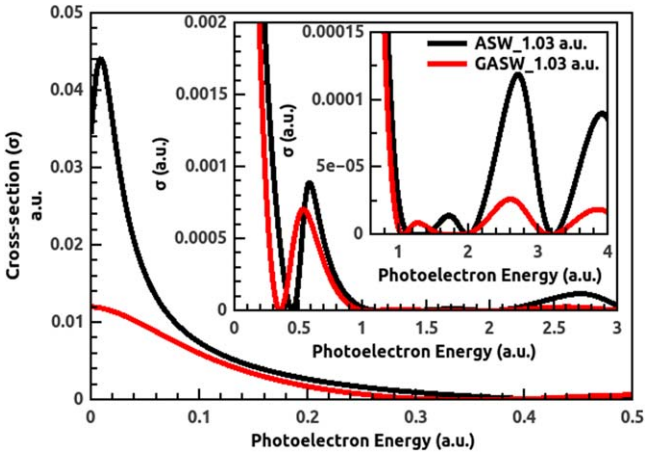

Figure 6. Comparison of photoionization cross-sections (σ) of $H@C_{60}$ for ASW and GASW confinements for the depth of 1.03 a.u. Enlarged versions of the cross-section at higher energies are given in insets.

Significantly different photoionization dynamics correspond to the strength of confinement seen for both ASW and GASW cases. A comparison of photoionization cross-sections of H for ASW and GASW confinements for the depth of 1.03 a.u. is shown in figure 6. The inset shows an enlarged view of the confinement oscillation in the cross-section, though with less amplitude. The origin of maxima and minima in the cross-section for the GASW potential depth of 1.03 a.u. will be analyzed in light of the product of the initial and final state wave functions. Figure 7 shows the initial state (u_{1s}) and final state ($u_{\varepsilon p}$) wave functions, and the product of these states ($u_{1s} \cdot u_{\varepsilon p}$) for V_{GASW} (r_c) = 1.03 a.u., corresponding to minima in the cross-section at $E_{PE} = 0.3532$ a.u. and 1.0564 a.u. and maxima at $E_{PE} = 0.5363$ a.u. and 1.2713 a.u. Note that for this particular depth, minimum points in the cross-section are actually zeros. From figure 7, it is seen that the minimum in the cross-section appears when the continuum wave function has either a maximum or minimum at the maximum of the initial wave function (figures 7(a) and (b)). At the same time, the maximum in the cross-section appears when the continuum wave function has some near-zero value at the maximum of the initial wave function (figures 7(c) and (d)). This observation does not agree with the conclusions made by Connerade *et al* [42]. Our observations show that there is no universal behavior for the origin of the minimum and maximum of the confinement oscillation; instead, it occurs as the overlap integral is flipped between the positive and negative sides. As the energy of the photon is increased, more maxima and minima will appear in the cross-section. The above analysis was carried out for an initial state and final state corresponding to the 1.03 a.u. depth of the GASW potential.

For smaller well depths, the initial state electron density is only partially transferred to the shell region (figures 2, 5). As a result, the nuclear region will also contribute to the overlap, which forces the minimum in the cross-section to not be at zero. This justification is consistent with our observation that the confinement oscillation is increased as the depth of the potential is increased. However, the mellowed oscillation in the GASW cross-section is in contrast with the oscillation in the ASW cross-section. This is due to the fact that the GASW confinement extends from the nuclear region to the border of the active region. On the contrary, the ASW confinement is strictly localized between $r_c - \frac{\Delta}{2}$ and $r_c + \frac{\Delta}{2}$. These differences in the potential modify both the initial and final state wave functions, and in turn affect the nature of the cross-section.

Since the atoms we have chosen for this study are light, there is a possibility that the confined atom can wiggle around inside the confining cage at any non-zero temperature. If the confined atom moves around inside the confining cavity, the partial waves become 'smeared out'. As a result, the associated interference oscillations can be mellowed in the cross-section, phase shift, and time delay. As we have seen from figures 3, 6, and 8, the primary effect of the GASW model potential is the mellowing down of the oscillations. In a sense, the smearing out of oscillations due to the wiggly motion can be accommodated by choosing a suitably soft spherically averaged confining potential. However, for larger atoms, the possibility of smearing out due to this phenomenon is less. Consequently, the degree of diffuseness and compactness of the GASW model potential needs to be tuned to address this situation.

Figure 8 shows the photoionization phase shift and time delay in both confinement cases for depths of 0.46 a.u. and 1.03 a.u. Confinement oscillations are seen in the phase shift

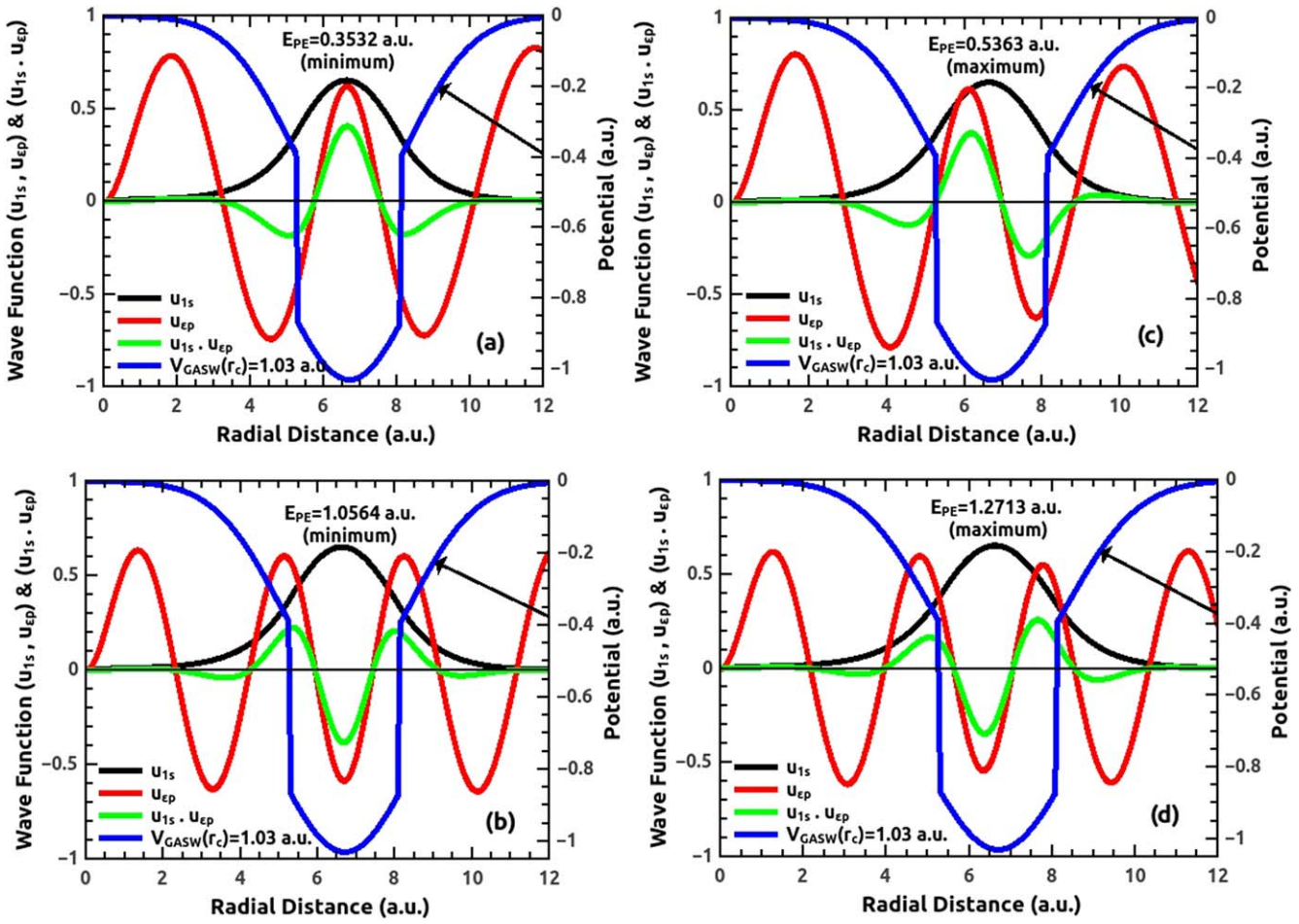

Figure 7. Initial state wave function (u_{1s}) and final state wave function ($u_{\varepsilon p}$) of the H@C_{60} atom, and the product of these states ($u_{1s} \cdot u_{\varepsilon p}$), for the 1.03 a.u. GASW, corresponding to minima at (a) $E_{PE} = 0.3532$ a.u. and (b) 1.0564 a.u., and maxima at (c) $E_{PE} = 0.5363$ a.u. and (d) 1.2713 a.u.

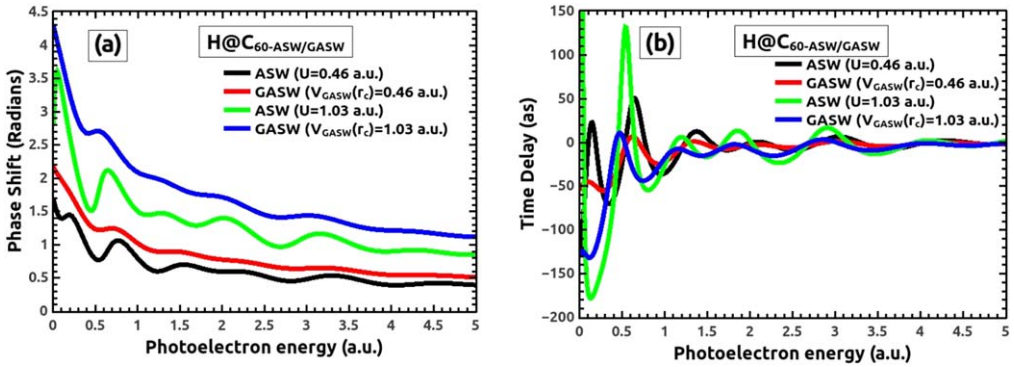

Figure 8. Comparison of (a) phase shift and (b) time delay of H@$V_{ASW/GASW}$ 1s photoionization for the confining potential depths of 0.46 a.u. and 1.03 a.u.

and time delay in both ASW and GASW confinement cases. It is known that the phase shift will decrease to zero as the photon energy is increased. Moreover, the phase shift increases as the depth of the potential is increased. This trend can be understood from the perspective of scattering, as the photoionization can be considered as half scattering [43]. The photoelectron that is released postinteraction is scattered more as the depth of the potential is increased. The signature of scattering is encoded in the phase shift; therefore, the phase shift is increased as the depth of the potential is increased. This behavior is consistent for ASW and GASW cases.

In addition, the photoelectron C_{60} in the GASW model experiences more scattering, which is due to the extended potential region of the GASW confinement. Because of this, as we see from figure 8(a), that GASW phase shift is slightly greater than that of the ASW. Oscillations in the GASW

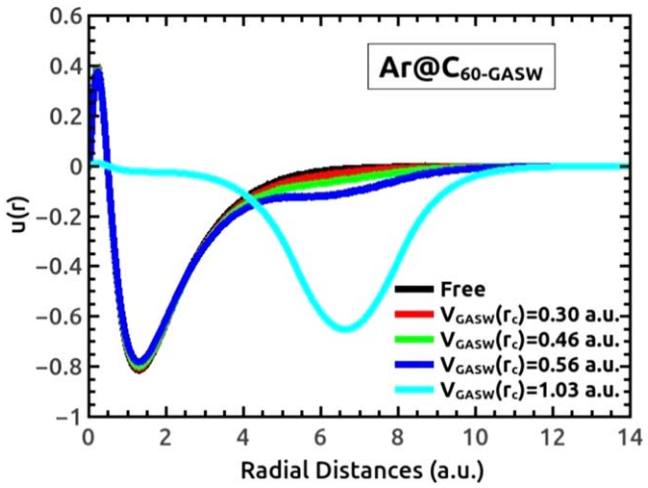

Figure 9. Radial wave function of the 3p electron of confined Ar for different depths of the GASW potential.

phase shift are smoothed compared to the ASW phase shift. In other words, the ASW phase shift is significantly modulated by the confinement oscillation compared to the GASW phase shift. The conclusion we have drawn in the context of oscillations in the cross-section can also be extrapolated to the phase shift. Since the GASW potential only partly brings the electron density to the shell region, the oscillations in the phase shift are slightly relaxed compared to the ASW case. Changes in the phase shift are extended into the time delay as well since the time delay is the energy derivative of the phase shift. Figure 8(b) shows that the time delay is dramatically affected due to confinement near the threshold. When the photoelectron energy is less, the outgoing electron spends more time near the confinement region to perceive finer details of the form of the potential. This will be culminated into significant changes in the time delay due to different forms of the confinement. For instance, ASW and GASW confinement near the threshold offers quite a different time delay for H-1s photoionization; at a depth of 1.03 a.u., the time delay at the threshold is positive for the ASW case whereas it is negative for the GASW case. Due to the changes in the confinement oscillations in the ASW and GASW phase shifts, the difference in the time delay is more amplified. This suggests that although the photoionization cross-section is qualitatively the same in the different confinement cases, the time delay is quite sensitive to the details of the potential. Since the time delay in photoionization is experimentally obtained, it is the quantity to be compared in search of the appropriateness of different model potentials. For a high photoelectron energy, photoionized electrons scatter very quickly. As a result, oscillations in the cross-section and phase shift would decay and the time delay go to zero. We see that both model potentials predict very different oscillations in the time delay not only near the threshold but also throughout the energy region considered. This observation demands more attention and experimental verification since we search for the realistic potential.

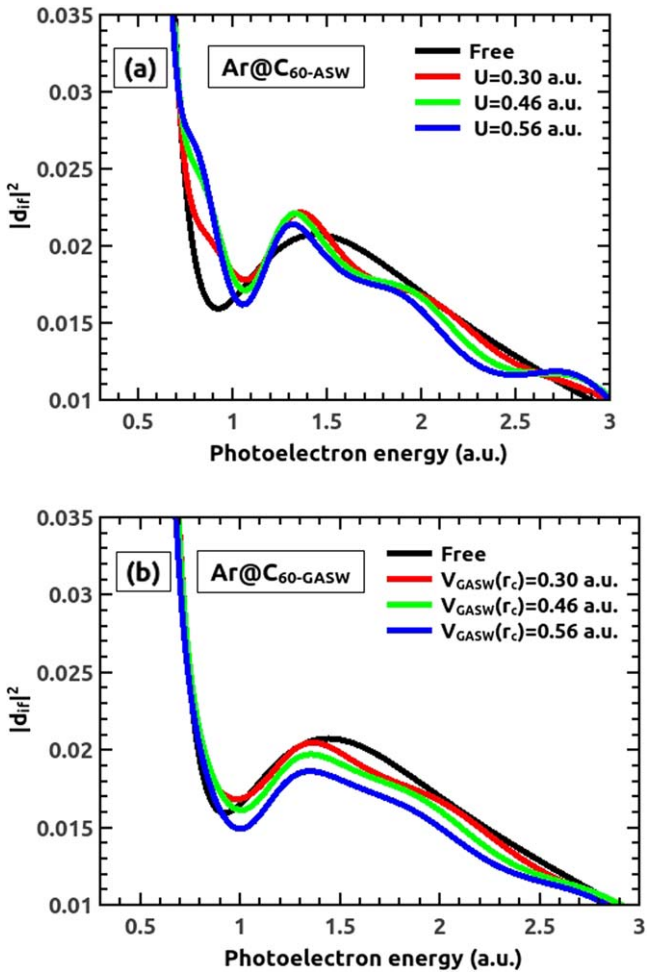

Figure 10. Absolute square of the dipole matrix element ($|d_{if}|^2$) of $Ar@C_{60}$ with (a) ASW confinement and (b) GASW confinement for different depths.

3.2. Photoionization from Ar@C60

Figure 9 shows the 3p wave function of confined Ar using the GASW model potential. This figure also compares the confined Ar results with the free case. Analogous to the case of H, confinement transfers electron density to the shell region. As the depth is increased to V_{GASW} $(r_c) = 1.03$ a.u., the electron density is completely transferred to the shell region. The effect of this on the photoionization dynamics is discussed below.

Figures 10(a) and (b) show the absolute square of the total dipole matrix element ($|d_{if}|^2$) of Ar under confinement modeled by the ASW and GASW potentials. Note that $|d_{if}|^2$ is proportional to the total photoionization cross-section (equation (11)). The figure shows the behavior of $|d_{if}|^2$ as the depth of confinement is increased; as expected, there are confinement oscillations similar to those in the case of photoionization of confined H. The $|d_{if}|^2$ is significantly modulated in the case of ASW confinement compared to GASW confinement. The mellowing down of oscillations in the cross-section in the GASW case is also quite consistent with the case of photoionization from confined H. The amount of modulation is seen to be enhanced as the depth is increased.

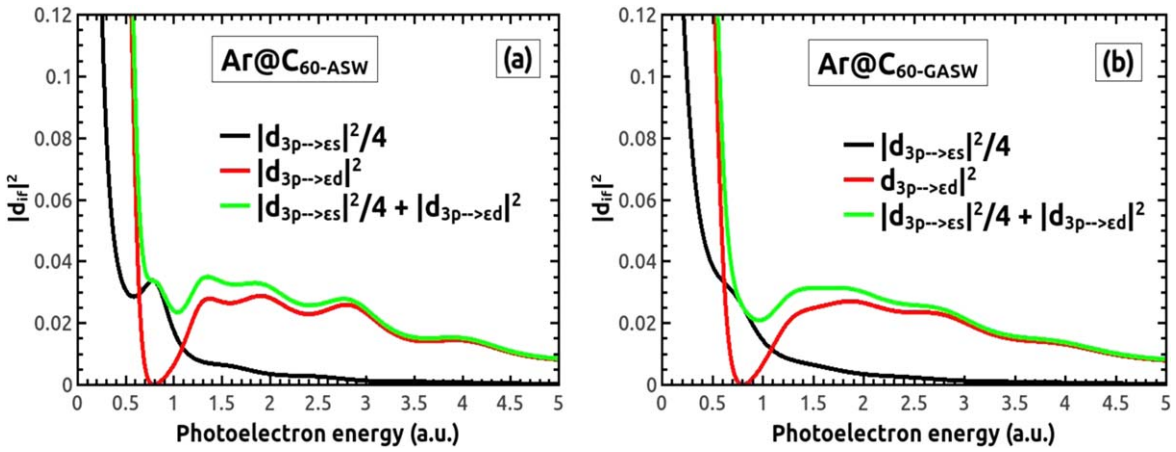

Figure 11. Absolute square of individual dipole matrix elements $3p \rightarrow \varepsilon s$ and $3p \rightarrow \varepsilon d$ and total dipole matrix element for (a) V_{ASW} (r_c) = 0.56 a.u. and (b) V_{GASW} (r_c) = 0.56 a.u.

Valance shell photoionization of noble gas atoms results in a minimum in the cross-section, which is named the Cooper minimum [10, 11, 20]. This happens when the dipole matrix element goes through zero as the overlap integral of the initial and final state wave functions cancel each other out because of their nodal behavior. The Cooper minimum is observed in the cross-section of free Ar near the photoelectron energy $E_{PE} = 0.92$ a.u. The location of the Cooper minimum in the $3p \rightarrow \varepsilon d$ channel of the free Ar is consistent with earlier theoretical and experimental reports [20, 44, 45]. Encapsulation of Ar shifts the Cooper minimum to the higher-energy region. The GASW predicts the Cooper minimum at $E_{PE} = 0.98$ a.u. while the ASW predicts it at $E_{PE} = 1.165$ a.u. (figure 10). This means that the GASW places the Cooper minimum closer to the free Ar cross-section than the ASW; therefore, GASW confinement affects the location of the Cooper minimum relatively less than ASW confinement. Since there is a plethora of works on photoionization from Ar@C_{60} by various models, the changes in the Cooper minimum region due to confinement can be used as a benchmark for choosing a realistic potential between the ASW and GASW. Javani *et al* [20] reported photoionization from confined Ar using time-dependent DFT. This work is more realistic because the technique also includes many-electron correlation effects from the C_{60} shell. We see from the work of Javani *et al* [20] that the effect of confinement on the Cooper minimum is not as dramatic as that obtained in ASW calculations, but it is consistent with the GASW calculation. This suggests that the GASW model can be accepted as a more realistic confinement potential in comparison with ASW models.

Since the total cross-section is the overall effect of two dipole channels, the shifting of the Cooper minimum upon encapsulation is analyzed for a particular depth with the help of $3p \rightarrow \varepsilon d$ and $3p \rightarrow \varepsilon s$ dipole channels. Figure 11 shows the $3p \rightarrow \varepsilon d$, $3p \rightarrow \varepsilon s$ dipole channels and the total dipole contribution of confined Ar using ASW and GASW model potentials. Figures 11(a) and (b), respectively, show the effect of ASW and GASW confinements. The $3p \rightarrow \varepsilon d$ contribution dominates in the entire region except in the Cooper minimum location. When the $3p \rightarrow \varepsilon d$ matrix element goes to zero, the cross-section will have a Cooper minimum. Upon encapsulation, individual dipole matrix elements are severely modulated by confinement oscillations. ASW matrix elements are modulated to a higher degree than GASW ones. At the Cooper minimum of the 'd channel', the oscillations in the 's channel' are very dramatic, leading to a maximum in the 's channel' dipole matrix element. This results in a competition between the oscillating 's channel' and 'd channel', and thus the Cooper minimum in the total cross-section is shifted to the higher-energy region. In the case of GASW confinement, the matrix elements are mildly modulated by confinement oscillations. Hence, GASW confinement does not significantly shift the Cooper minimum compared ASW confinement.

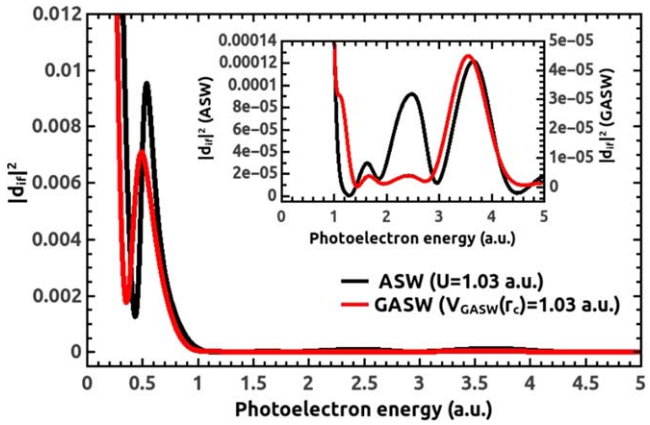

Figure 12. Comparison of photoionization cross-sections of Ar@C_{60} for ASW and GASW confinement for the depth of 1.03 a.u. An enlarged version of the cross-section at higher energies is given in the inset.

Another interesting observation is that the cross-section at the Cooper minimum decreases as the depth of confinement increases. This behavior is analyzed with the help of numerical values of the individual dipole channel contribution ($3p \rightarrow \varepsilon d$ and $3p \rightarrow \varepsilon s$) at the Cooper minimum (table 2).

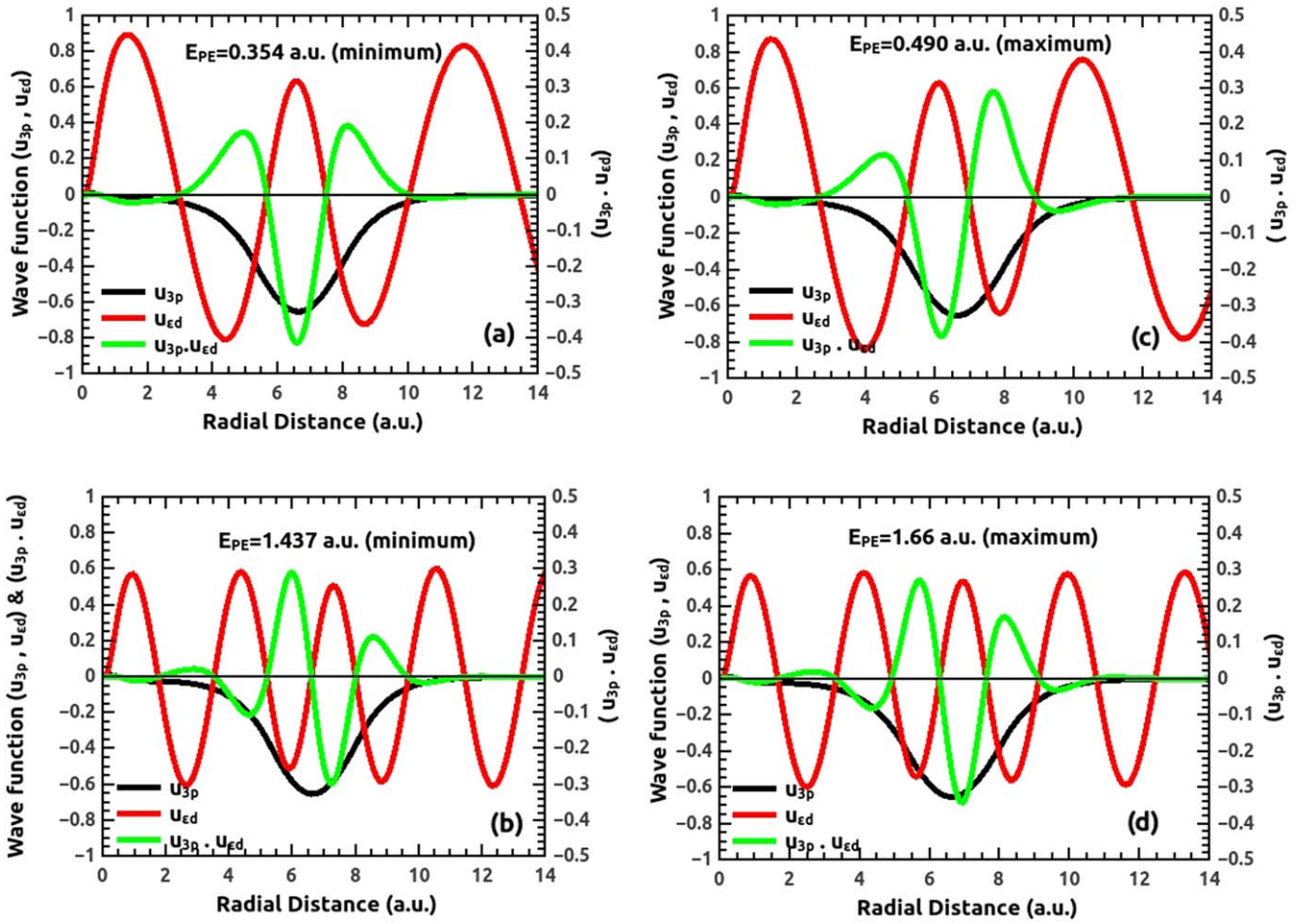

Figure 13. Initial state (u_{3p}), final ($u_{\varepsilon d}$) state, and product of the states ($u_{1s} \cdot u_{\varepsilon p}$) for Ar@$C_{60\text{-GASW}}$ with the depth of 1.03 a.u., corresponding to minima at (a) $E_{PE} = 0.354$ a.u. and (b) 1.437 a.u., and maxima at (c) $E_{PE} = 0.490$ a.u. and (d) 1.66 a.u.

Table 2. Dipole matrix elements of $3p \rightarrow \varepsilon s$ and $3p \rightarrow \varepsilon d$ channels at the Cooper minimum location for the ASW case. Entries in parentheses are for the GASW case.

Depth (a.u.)	$\langle 3p\|r\|\varepsilon s\rangle$ ASW (GASW)	$\langle 3p\|r\|\varepsilon d\rangle$ ASW (GASW)
0	0.276	0.058
0.30	0.255	0.099
	(0.269)	(0.07)
0.56	0.239	0.096
	(0.242)	(0.080)

One can see that the $3p \rightarrow \varepsilon s$ contribution decreases as the depth increases, which decreases the whole cross-section amplitude at the Cooper minimum. This behavior is similar for both ASW and GASW cases. However, in GASW confinement, the $3p \rightarrow \varepsilon s$ dipole contribution is less affected.

Note that in the above comparison of the cross-section, the confinement depth of 1.03 a.u. was omitted. This is in view of the fact that the initial wave function corresponding to a depth of 1.03 a.u. is completely transferred to the well region, as shown in figure 9. This will result in significantly different photoionization dynamics for ASW and GASW cases.

Figure 12 shows a comparison of the photoionization cross-sections of Ar for ASW and GASW confinements for the depth of 1.03 a.u. The nature of the cross-section corresponding to this depth is significantly different from those of other confinement depths considered earlier. This is consequent with the mirror collapse with the 4p excited state. The photoionization cross-section has a prominent peak at ∼0.6 a.u. in both cases of confinement. However, the ASW cross-section is marginally higher than the GASW counterpart. At higher energies, there are confinement oscillations in the cross-section, though with small amplitude. The magnified version of the cross-section in the high-energy region is shown in the inset of figure 12. The oscillations in the cross-section are mild in the GASW compared to those in the ASW. The previous analysis of the origin of maxima and minima in the cross-section is repeated for the case of Ar photoionization. It is done with the help of minima at $E_{PE} = 0.354$ a.u. and 1.437 a.u. and maxima in the cross-section at $E_{PE} = 0.490$ a.u. and 1.66 a.u. for the 1.03 a.u. depth of the GASW confinement (figure 12). Since the contribution of the $3p \rightarrow \varepsilon d$ channel is more prominent at these maxima and minima points, we show in figure 13 the initial state wave function (u_{3p}), final state wave function ($u_{\varepsilon d}$), and product of the states ($u_{1s} \cdot u_{\varepsilon p}$). It can be seen that the minimum in the

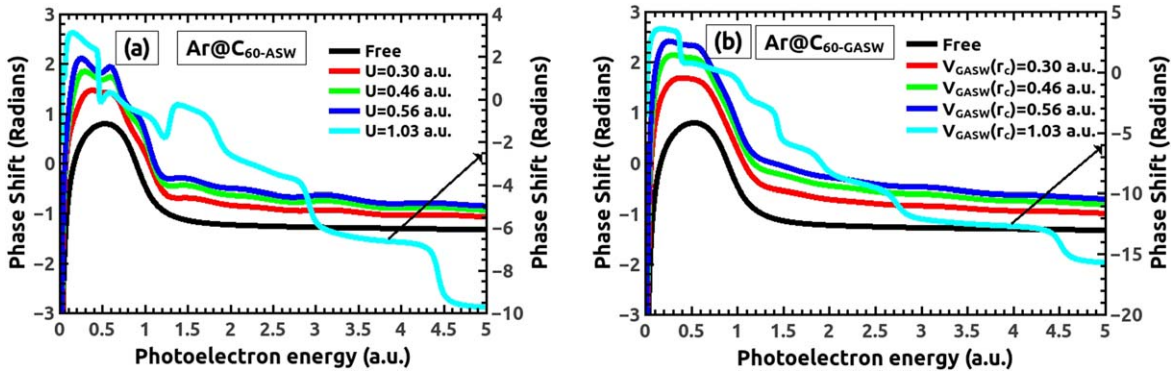

Figure 14. Total dipole phase of Ar 3p photoionization for different strengths of confinement using (a) ASW and (b) GASW models.

cross-section occurs when the continuum wave function goes through a nodal point or has a maximum/minimum at the peak position of the initial state wave function and a maximum when the continuum wave function has some near-zero value just around the peak position of the initial state wave function. As the photon energy is increased, more maxima and minima will appear in the cross-section. This observation is in line with that found in the photoionization from H, where there is no universal behavior one can attribute to the minima and maxima in the confinement oscillations.

Figures 14(a) and (b) show the variation of the photoionization phase shift of Ar for both confinement cases as the depth of the confinement is increased. The dipole phase of the free Ar photoelectron shows a dramatic jump of about 2 radians near the Cooper minimum. Consequent to the shift of Cooper minimum location in confined Ar, energy at which phase jump occurs is also moved up. However, the phase jump due to the Cooper minimum is modulated by confinement oscillations in both confinement cases. In both ASW and GASW cases, the phase shift increases as the depth of the potential increases. Like in the case of the cross-section, the phase shift corresponding to a depth of 1.03 a.u. shows interesting dynamics. The phase shift is dominated by confinement oscillations. This dramatic change is due to the significant changes in the initial state and continuum state wave function at this potential depth. We notice several jumps in the phase shift at minima in the cross-section. Note that at V_{GASW} $(r_c) = 1.03$ a.u., most of the initial state electron density is transferred to the shell region. Therefore, the confinement oscillations will happen at full throttle, which makes the dipole matrix element go through zero. The transition of the dipole matrix element through zero results in a sharp jump in phase shift. This behavior is quite similar to what happens to the phase shift at the Cooper minimum. Note however that these jumps are not abrupt in the confinement cases outside of the depth of 1.03 a.u., but are visible as smooth oscillations.

A smaller well depth ensures only partial transfer of electron density to the shell region; therefore, confinement oscillations are not very dramatic. As a result, the nuclear region will also contribute to the overlap, which forces the minimum in the cross-section to not be zero. This justification is quite consistent with the observations made in the case of H photoionization. Clearly, this is the first report about confinement oscillations inducing jumps in the dipole phase just as in the case of the Cooper minimum.

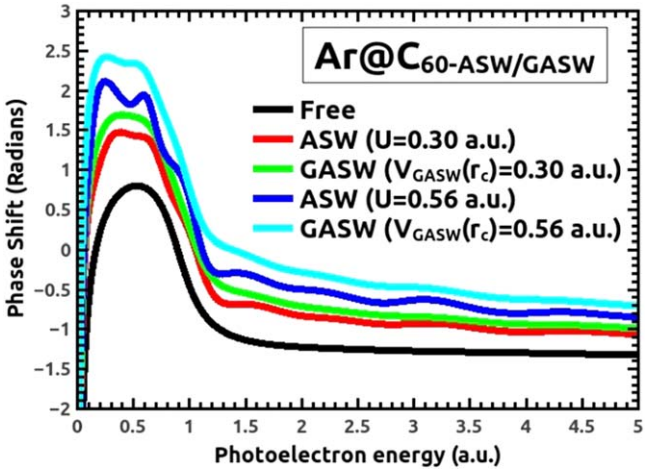

Figure 15. Comparison between total dipole phases of confined Ar using ASW and GASW model potentials.

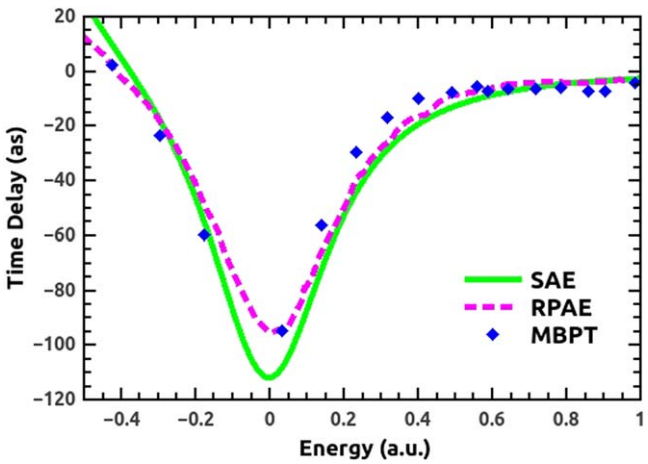

Figure 16. Comparison of the photoionization time delay of the 3p subshell of free Ar using the SAE model potential (equation (7)), with RPAE [11] and MBPT [46] results with respect to the location of the Cooper minimum.

Figure 15 compares the ASW and GASW phases of the dipole matrix element for two different depths of confinement.

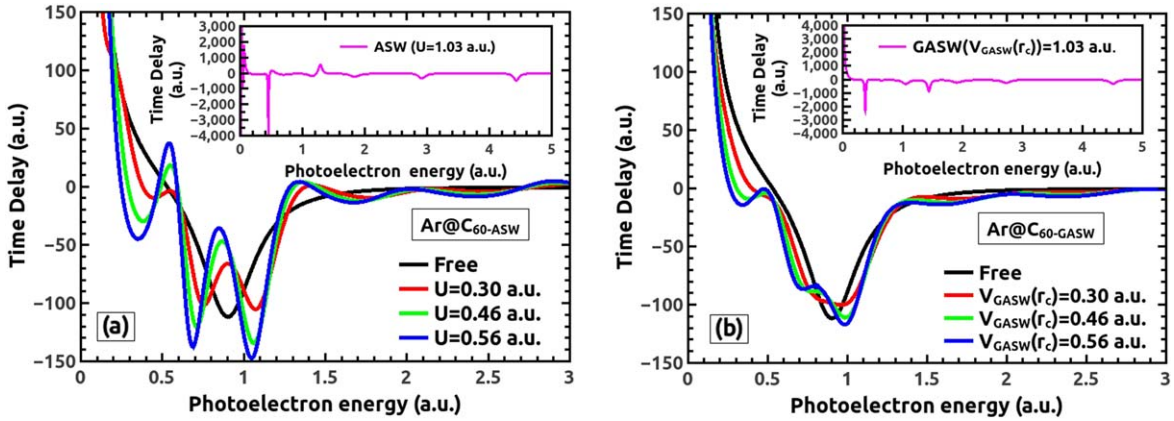

Figure 17. Time delay in Ar 3p photoionization with different strengths of confinement using (a) ASW and (b) GASW models.

Like in the case of H photoionization, the dipole phase of the GASW case is slightly greater than that of the ASW and the oscillation is more mellowed. This is due to the extended behavior of the GASW over the entire region. Because of this, the phase shift due to the GASW confinement contributes at each and every radial point in the active region, not only within the localized confinement boundary between $r_c - \frac{\Delta}{2}$ and $r_c + \frac{\Delta}{2}$ like in the ASW.

In figure 16, the time delay in Ar 3p photoionization using the SAE model is compared with the nonrelativistic random phase approximation (RPAE) [11] and many-body perturbation theory (MBPT) [46] results, with reference to the location of respective Cooper minima. The present work shows that the SAE model predicts a time delay comparable to that predicted by RPAE and other many-body methods. Photoionization from free Ar shows considerable time delay (−110 as) at the position of the Cooper minimum. This case is well studied, employing sophisticated many-electron techniques [46]. For free Ar, the weak transition $3p \rightarrow \varepsilon s$ takes over near the Cooper minimum of the strong $3p \rightarrow \varepsilon d$ transition, and the resulting time delay does not go below −110 as. This value is in good agreement with the result predicted by RPAE [11]. However, the SAE model potential predicted a somewhat deeper time delay at the Cooper minimum [10]. Agreement between RPAE result and the present result shows that the −110 as time delay at the Cooper minimum is mostly contributed by the screening effect, which is present in both types of calculations. In other words, the correlation effects in the RPAE calculation does not offer many significant changes in the time delay at the Cooper minimum. This analysis is vital, and shows that the time delay is realistically contributed by the screening effect, not by the correlation and other effects. A similar observation was already made in [46] using a single active orbital approximation. The two model potentials predict very different oscillations in time delay.

At low photoelectron energies, slight changes in the confinement oscillations in the ASW and GASW phases induce a significant difference in the time delay. Evidently, oscillations furnished by GASW confinement are smoother than those in the ASW case. The depth of 1.03 a.u. offers a dramatically different time delay since the phase is also significantly different; this is shown in the inset of figure 17. Corresponding to every jump in the phase, a jump in the time delay in the negative direction is seen.

Figures 17(a) and (b) show the time delay in the photoionization of confined Ar modeled by the ASW and GASW for three different depths. Mellowed confinement oscillation is evident in the latter case. This analysis also confirms that the time delay in photoionization is extremely sensitive to the details of the confining potential, and therefore this parameter could be considered as a benchmark for choosing the right potential.

4. Conclusions

A systematic study of the effects of confinement by fullerene on the photoionization dynamics of H and Ar is performed in this work. The photoionization calculations are done in an SAE approximation to isolate the effects of confinement from other correlation effects. The endohedral confinement is modeled by compact (ASW) and diffused (GASW) potentials, and therefore their contrasting effects on the photoionization parameters are elucidated. In search of a realistic potential to mimic C_{60} confinement, the smooth edges and nonflat bottom of the GASW potential provide an advantage over the square well-type model potential.

A detailed study of the origin of confinement oscillations revealed that there is no universal behavior that can be attributed to the minimum and maximum in the oscillating cross-section. GASW confinement results in a mild modulation over the free photoionization parameters whereas ASW confinement facilitates strong oscillations.

In $Ar@C_{60}$, the Cooper minimum shifts to a higher energy. The degree of this shifting is much less in GASW cases compared to ASW confinement. Confinement oscillations of the cross-section of $Ar@C_{60}$ are appreciably consistent with the self-consistent field DFT calculation, which suggests that when looking for a realistic potential to mimic confinement, the GASW model is definitely a potential candidate with the right amount of diffuseness and compactness.

In the case of photoionization from Ar, confinement oscillations at the well depth of 1.03 a.u. seem to behave analogously to the Cooper minimum, exhibiting sharp jumps in the dipole phases. This is, to the best of our knowledge, the first report connecting the Cooper minimum and confinement oscillation from the perspective of dipole phases. Furthermore, confinement effects on the phase shift are amplified in the photoionization time delay. Near the threshold, the time delay exhibits stronger sensitivity to the details of the confining potential. This shows that an experimentalist can consider the atomic photoionization time delay as a potential candidate for judging the reliability of any confinement model potential. Our SAE model predicted a time delay at the Cooper minimum location quite comparable to the one predicted by RPAE [11], which suggests that correlation effects contribute the least to the time delay (compared with the screening effect near the Cooper minimum region).

In summary, this work showcased the confinement effects of photoionization parameters such as the transition dipole, phase shift, and time delay. In the search for a confinement potential with the right amount of diffuseness and compactness, our comparison shows that the GASW is a potential choice.

Acknowledgments

J J acknowledges the support provided by SERB through project no. ECR/2016/001564, and HRV is supported by the DST-SERB, India under grant no. EMR/2016/002695. The authors are grateful to Dr Anh-Thu Le for helpful discussions. We are thankful to the referees of this article for very constructive criticisms.

ORCID iDs

Hari R Varma https://orcid.org/0000-0001-9072-0041
Jobin Jose https://orcid.org/0000-0002-8534-8473

References

[1] Harneit W, Boehme C, Schaefer S, Huebener K, Fostiropoulos K and Lips K 2007 *Phys. Rev. Lett.* **98** 216601
[2] Melanko J B, Pearce M E and Salem A K 2009 *Nanotechnology in Drug Delivery* ed M M de Villiers *et al* (New York: Springer) p 105
[3] Ross R B *et al* 2009 *Nat. Mater.* **8** 208
[4] Nierengarten J-F 2004 *New J. Chem.* **28** 1177–91
[5] Kang J W and Hwang H J 2004 *Nanotechnology* **15** 614–21 Institute of Physics Publishing
[6] Takeda A *et al* 2006 *Chem. Commun.* **8** 912
[7] Da Ros T, Spalluto G and Prato M 2001 *Croat. Chem. Acta* **74** 743–55 https://hrcak.srce.hr/131951
[8] Zadik R H *et al* 2015 *Sci. Adv.* **1** e 1500059
[9] Zhao Y, Kim Y H, Dillon A C, Heben M J and Zhang S B 2005 *Phys. Rev. Lett.* **94** 155504
[10] Saha S, Mandal A, Jose J, Varma H R, Deshmukh P C, Kheifets A S, Dolmatov V K and Manson S T 2014 *Phys. Rev.* A **90** 053406
[11] Kheifets A S 2013 *Phys. Rev.* A **87** 063404
[12] Klüunder K *et al* 2011 *Phys. Rev. Lett.* **106** 143002
[13] Dolmatov V K, Baltenkov A S, Connerade J-P and Manson S T 2004 *Radiat. Phys. Chem.* **70** 417–33
[14] Phaneuf R A *et al* 2013 *Phys. Rev.* A **88** 053402
[15] Connerade J P, Dolmatov V K, Lakshmi P A and Manson S T 1999 *J. Phys. B: At., Mol. Opt. Phys.* **32** L239
[16] Bransden B H and Joachain C J 2003 *Physics of Atoms and Molecules* (India: Pearson Education)
[17] Landau L D and Lifshitz E M 1965 *Quantum Mechanics: Non-relativistic Theory* (Oxford: Pergamon)
[18] Amusia M Y, Baltenkov A S, Chernysheva L V, Felfli Z and Msezane A Z 2005 *J. Phys. B: At., Mol. Opt. Phys.* **38** L169–73
[19] Amusia M Y, Chernysheva L V and Dolmatov V K 2011 *Phys. Rev.* A **84** 063201
[20] Javani M H, Chakraborty H S and Manson S T 2014 *Phys. Rev.* A **89** 053402
[21] Nascimento E M, Prudente F V, Guimarães M N and Maniero A M 2011 *J. Phys. B: At., Mol. Opt. Phys.* **44** 015003
[22] Dolmatov V K, King J L and Oglesby J C 2012 *J. Phys. B: At., Mol. Opt. Phys.* **45** 105102
[23] Baltenkov A S, Manson S T and Msezane A Z 2015 *J. Phys. B: At., Mol. Opt. Phys.* **48** 185103
[24] Patel A B and Chakraborty H S 2011 *J. Phys. B: At., Mol. Opt. Phys.* **44** 191001
[25] Puska M J and Nieminen R M 1993 *Phys. Rev.* A **47** 1181
[26] Gorczyca T W, Hasoglu M F and Manson S T 2012 *Phys. Rev.* A **86** 033204
[27] Connerade J P, Dolmatov V K and Manson S T 1999 *J. Phys. B: At., Mol. Opt. Phys.* **32** L395
[28] Varma H R, Deshmukh P C, Dolmatov V K and Manson S T 2007 *Phys. Rev.* A **76** 012711
[29] Winstead C and McKoy V 2006 *Phys. Rev.* A **73** 012711
[30] Dolmatov V K, Amusia M Y and Chernysheva. L V 2015 *Phys. Rev.* A **92** 042709
[31] Rüdel A, Hentges R, Becker U, Chakraborty H S, Madjet M E and Rost J M 2002 *Phys. Rev. Lett.* **89** 125503
[32] Madjet M E, Chakraborty H S, Rost J M and Manson S T 2008 *J. Phys. B: At., Mol. Opt. Phys.* **41** 105101
[33] Le A-T, Lucchese R R, Tonzani S, Morishita T and Lin C D 2009 *Phys. Rev.* A **80** 013401
[34] Tong X M and Lin C D 2005 *J. Phys. B: At., Mol. Opt. Phys.* **38** 2593–600
[35] Friedrich H 2005 *Theoretical Atomic Physics* (Berlin: Springer)
[36] Wigner E P 1955 *Phys. Rev.* **98** 145
[37] Joachain C J 1975 *Quantum Collision Theory* (Amsterdam: North-Holland)
[38] Kumar A, Varma H R, Deshmukh P C, Manson S T, Dolmatov V K and Kheifets A S 2016 *Phys. Rev.* A **94** 043401
[39] Lin C Y and Ho Y K 2012 *J. Phys. B: At., Mol. Opt. Phys.* **45** 145001
[40] Martínez-Flores C and Cabrera-Trujillo R 2018 *J. Phys. B: At., Mol. Opt. Phys.* **51** 055203
[41] Jose J, Pradhan G B, Radojević V, Manson S T and Deshmukh P C 2011 *J. Phys. B: At., Mol. Opt. Phys.* **44** 195008
[42] Connerade J P, Dolmatov V K and Manson S T 2000 *J. Phys. B: At., Mol. Opt. Phys.* **33** 2279–85
[43] Fano U and Rau A R P 1986 *Atomic Collisions and Spectra* (London: Academic)
[44] Johnson W R and Cheng K T 1979 *Phys. Rev.* A **20** 978
[45] Marr G V and West J B 1976 *At. Data Nucl. Data Tables* **18** 497
[46] Dahlström J M, Carette T and Lindroth E 2012 *Phys. Rev.* A **86** 061402 (R)